

Three-Dimensional Nanocharacterization of Porous Hydrogel With Ion and Electron Beams

Aswan Al-Abboodi,¹ Jing Fu,² Pauline M. Doran,³ Peggy P.Y. Chan^{4,5}

¹Department of Chemical Engineering, Monash University, Clayton, VIC, Australia

²Department of Mechanical and Aerospace Engineering, Monash University, Clayton, VIC 3800, Australia; telephone: +61 3 9905 3707; fax: +61 3 9905 1825;

e-mail: jing.fu@monash.edu

³Faculty of Life & Social Sciences, Swinburne University of Technology, Hawthorn, VIC, Australia

⁴School of Applied Science, RMIT University, Melbourne, VIC, Australia; telephone: +61 3 9925 2660; e-mail: peggy.chan@rmit.edu.au

⁵Micro/Nanophysics Research Laboratory, RMIT University, Melbourne, VIC 3000, Australia

ABSTRACT: Porous hydrogels provide an excellent environment for cell growth and tissue regeneration, with high permeability for oxygen, nutrients, and other water-soluble metabolites through their high water-content matrix. The ability to image three-dimensional (3D) cell growth is crucial for understanding and studying various cellular activities in 3D context, particularly for designing new tissue engineering scaffold, but it is still challenging to study cell-biomaterial interfaces with high resolution imaging. We demonstrate using focused ion beam (FIB) milling, electron imaging, and associated microanalysis techniques that novel 3D characterizations can be performed effectively on cells growing inside 3D hydrogel scaffold. With FIB-tomography, the porous microstructures were revealed at nanometer resolution, and the cells grown inside. The results provide a unique 3D measurement of hydrogel porosity, as compared with those from porosimetry, and offer crucial insights into material factors affecting cell proliferation at specific regions within the scaffold. We also proved that high throughput correlative imaging of cell growth is viable through a silicon membrane based environment. The proposed approaches, together with the protocols developed, provide a unique platform for analysis of the microstructures of novel biomaterials, and for exploration of their interactions with the cells as well.

Biotechnol. Bioeng. 2013;110: 318–326.

© 2012 Wiley Periodicals, Inc.

KEYWORDS: porous hydrogel; focused ion beam (FIB); SEM; tomography; cell growth

Introduction

Hydrogels are synthetic or natural polymer networks that have emerged as promising candidates for three-dimensional (3D) tissue engineering scaffolds with tissue-like stiffness and biocompatibility (da Silva et al., 2010). The use of macroporous hydrogels as scaffolds in tissue engineering is advantageous in supporting cell proliferation, migration, and tissue regeneration compared to non-porous hydrogels (Ford et al., 2006; Hollister, 2005; Keskar et al., 2009). It is increasingly recognized that pore size and density of cell binding ligands and other physical parameters such as topography are vital design variables for substrates used in tissue engineering and biochemical applications (Nehrer et al., 1997; Wang et al., 2010). The ability to image cell growth within the scaffold and how cell interact with the scaffold is crucial to the understanding and validation of hydrogel scaffold designs, but there are still several hurdles to overcome. Microtomy or ultramicrotomy, the standard method to prepare thin sections for transmission electron microscopy (TEM), is well known for issues when cutting materials of high heterogeneity. Due to the different physical natures of the cells and the surrounding biomaterials, there is a high risk of detachment of cells during microtome cutting, which prevents routine TEM imaging at cell-hydrogel interfaces (Edwards et al., 2009). Investigation using scanning electron microscopy (SEM) is restricted to the sample surface, as the detection depth is limited by the interaction volume of the electrons and is typically only a

Additional supporting information may be found in the online version of this article. The authors declare no conflict of interest.

Correspondence to: J. Fu and P. P.Y. Chan

Contract grant sponsor: Australian Research Council Discovery (ARC) Project Grant

Contract grant number: DP 120102570; DP 120100583

Received 30 May 2012; Revision received 8 July 2012; Accepted 10 July 2012

Accepted manuscript online 18 July 2012;

Article first published online 6 August 2012 in Wiley Online Library

(<http://onlinelibrary.wiley.com/doi/10.1002/bit.24612/abstract>)

DOI 10.1002/bit.24612

few micrometers. In terms of porosity characterization, confocal microscopy offers a straightforward solution for imaging cells in hydrogel supported by fluorescence staining. General characteristics such as porosity and cell viability can be obtained, but the resolution is still restricted without the capability to resolve subtle morphology such as focal adhesions (FAs) at the interfaces. Other indirect approaches for porosity measurement, such as mercury intrusion porosimetry and the gas expansion method, provide only the average measurements for the whole sample without considering spatial variations. High resolution 3D investigation of cells in a matrix is still challenging due to the lack of appropriate tools and protocols.

Recently, focused ion beam (FIB) technology and associated microanalysis methods, which were developed originally for applications in materials science, have emerged in biomedical fields. Using these techniques, an ultrafine beam of accelerated ions, typically gallium or helium, can be directed to a region of interest on the target surface, with the size of the focused beam reduced to only a few nanometers (Giannuzzi and Stevie, 2005; Volkert and Minor, 2007). The actual mechanism of interaction between the accelerated particles and the target solid is complicated; however, for steps used in this study, atomic collision referred to as sputtering is the dominant phenomenon. Nano/microscale volumes can be removed in a controlled manner and numerous applications have been enabled, such as nanopore fabrication for DNA analysis (Li et al., 2001). For some biomaterials, such as bone, that present difficulties for microtome sectioning, FIB has begun to serve as the unique solution for preparing thin sections for TEM investigations (Lucille et al., 2007). With advances in automation and control, focused ion, and electron beams can be applied alternately to remove a thin layer of sample followed by electron image acquisition. This “slice and image” approach (FIB-tomography used in this manuscript), also referred to as FIB/SEM tomography or ion abrasion SEM (IA-SEM), allows 3D reconstruction of intracellular and intercellular ultrastructures with the captured serial SEM images. The thickness of each layer can approach 10 nm, and the resolution of stained cells with current SEMs is sufficient to reveal various organelles and membranes. Recent applications of these techniques include reconstructions of yeast cells (Heymann et al., 2006), chromosomes (Schroeder-Reiter et al., 2009), diatoms (Hildebrand et al., 2009), mammalian cells (Heymann et al., 2009; Knott et al., 2008), and even HIV virological synapses (Bennett et al., 2009; Felts et al., 2010).

The unique capabilities of FIB offer the promise of 3D characterization of cells and their surrounding biomaterials. Initial attempts have been presented (Bittermann et al., 2009; Friedmann et al., 2011b; Martínez et al., 2008), in which FIB milling was applied to expose the cell–material interfaces, or intracellular nanoparticles (Friedmann et al., 2011a; Greulich et al., 2011). In this study, we perform the first 3D investigation of cells grown in hydrogel scaffold using FIB milling and associated microanalysis techniques.

The acquired information, particularly the 3D reconstructions that are difficult to obtain using other approaches, provide a unique 3D measurement of the porous microstructures as well as details of the cell morphology.

Materials and Methods

Materials

Gelatin (Gtn) ($M_w = 80\text{--}140$ kDa, $pI = 5$) and horseradish peroxidase (HRP) (100 units/mg) were obtained from Wako Pure Chemical Industries (Novachem Pty Ltd, Collingwood, Australia). 3,4-Hydroxyphenylpropionic acid (HPA), *N*-hydroxysuccinimide (NHS), 1-ethyl-3-(3-dimethylaminopropyl)-carbodiimide hydrochloride (EDC.HCl), carboxymethyl cellulose (CMC) ($M_w = 90$ kDa), and tyramine hydrochloride (Tyr) were purchased from Sigma–Aldrich (Australia). Fetal bovine serum (FBS), 4',6-diamidino-2-phenylindole (DAPI), and fluoresceinamine isomer I were provided by Invitrogen (Life technologies Australia Pty Ltd, Mulgrave, Australia). *N,N*-Dimethylformamide (DMF) and hydrogen peroxide (H_2O_2) were acquired from Merck (Merck Pty Ltd, Kilsyth, Australia).

Preparation of Scaffold Conjugates

Gtn–HPA conjugates were prepared as described in (Lee et al., 2006) by a general carbodiimide/active ester-mediated coupling reaction in distilled water. Briefly, HPA (3.32 g) was dissolved in 250 mL of a 3:2 (v/v) mixture of distilled water and DMF. To this solution, NHS (3.20 g) and EDC.HCl (3.82 g) were added. The mixture was stirred at room temperature for 5 h at pH 4.7 and room temperature. Then, 150 mL of a 6.25 wt% aqueous solution of Gtn was added and the mixture was stirred overnight at room temperature and pH 4.7. The solution was transferred to dialysis tubes with a molecular cut-off of 1,000 Da. The products were dialyzed against 100 mM NaCl, 25% ethanol, and MilliQ water in sequence for 2 days each. The purified solution was lyophilized to obtain Gtn–HPA conjugates. To synthesize fluorescently labeled Gtn–HPA conjugates, the carboxylic acid groups were activated before adding fluoresceinamine isomer I (3.637 mg). CMC–Tyr conjugates were prepared by adding CMC (5 g) and Tyr (0.8648 g) to milliQ water (250 mL). To this solution, NHS (0.5732 g) and EDC.HCl (0.9547 g) were added immediately. The products were dialyzed and lyophilized in a similar manner as for Gtn–HPA.

Polymerization of the Gtn–HPA/CMC–Tyr Hydrogel Scaffold

Gtn–HPA/CMC–Tyr hydrogel scaffold was prepared by mixing 5% (w/v) Gtn–HPA and CMC–Tyr conjugate solutions using a weight ratio of 80:20, respectively. The

mixture was vortexed vigorously for a few minutes. The resulting polymer was polymerized using enzymatic oxidative coupling by adding HRP and diluted H₂O₂ at concentrations of 7.7 unit/L and 49.8 μM, respectively. This peroxidase mediated oxidative coupling process has been employed to crosslink Gtn-HPA and other phenol-containing polymers (Jin et al., 2010; Lee et al., 2008), and is known to yield biocompatible 3D hydrogels. This mixture was injected into plastic well plates, which represented the host in this study, and allowed to gel. Hydrogel with porous structure can be obtained via polymerization induced phase separation due to the difference in Gtn-HPA and CMC-Tyr hydrophobicity.

Cell Culture

African green monkey kidney cells (COS-7 cell line) were cultivated in Dulbecco's modified Eagle's medium (DMEM) supplemented with 10% (v/v) FBS, 100 μg/mL streptomycin, and 100 μg/mL penicillin at 37°C in a gassed incubator with 5% CO₂ before mixing with the scaffolds. All incubations were performed under these culture conditions. COS-7 cells at a density of 2×10^5 per T-flask were seeded 3 days before harvesting. When the cells were 80% confluent, the medium was removed, the cells were washed with PBS buffer, and trypsin was added to detach the cells for collection. The harvested cells were rinsed with medium.

Preparation of Scaffold Samples for Laser Scanning Confocal Microscopy

Porous hydrogel scaffolds polymerized from fluorescent Gtn-HPA/CMC-Tyr were investigated by laser scanning confocal microscopy (LSCM) imaging. A 0.1 mL aliquot of scaffold sample solution was pipetted on to a microscope slide after mixing with COS-7 cells and the solution was polymerized by adding HRP and H₂O₂. The slides were left at room temperature for 2 h for phase separation. A Nikon A1Rsi LSCM with a 60× water immersion lens (numerical aperture 1.00) was used to collect three images from random locations within each sample. A median filter was applied to each image to eliminate isolated erroneous pixels without modifying edges, and the contrast was then optimized by ignoring 3% of the brightest and darkest pixels and spreading the intensity range of the remaining pixels linearly to cover the maximum available value range. Cell pellets inside hydrogel scaffolds that were subjected to LSCM imaging were also observed using light microscopy by preparing some non-fluorescencelabeled scaffold samples.

Focal Adhesion Staining

FA kit Merck Millipore (Merck Ltd, Kilsyth, Australia) was used to stain the cell FA; cells were fixed with 4% paraformaldehyde, then rehydrated in PBS, permeabilized with 0.1% Triton X-100, and blocked with 1% BSA in PBS.

After washing with PBS containing 0.05% Tween-20 (washing buffer), cells were incubated with primary antibody (anti-Vinculin) diluted in blocking solution (1% BSA in 1× PBS) for 1 h at room temperature then washed with washing buffer. Secondary antibodies (antimouse IgG conjugated with alexa-fluor-488 or -568) were applied for 1 h and TRITC conjugated phalloidin was incubated with the secondary antibody for double labeling. Finally, DAPI stain was performed following the last washing step to stain the nuclei.

Preparation of SEM Samples

For environmental SEM (ESEM) imaging, hydrogel scaffold samples maintained in a hydrated state with or without cells were transferred directly to the instrument for imaging. For other SEM investigations, hydrogel precursors were sterilized and mixed with COS-7 cell pellets before polymerization using HRP and H₂O₂. Both the cell-seeded and cell-free scaffolds, once gelled on microscope slides, were frozen rapidly by plunging into liquid nitrogen (approximately -196°C) and then freeze-dried for 2 days for vacuum-based analysis. Additional aliquots for high resolution imaging were stained with osmium tetroxide (OsO₄). Cells inside the scaffolds were fixed with 2.5% glutaraldehyde in 100 mM sodium cacodylate buffer, pH 7.4, for 4 h, and stored at 4°C overnight. Cells were washed three times for 5 min each in 100 mM sodium cacodylate buffer. The samples were then treated for 1 h with 2% OsO₄ reduced with 1.5% potassium ferrocyanide. After rinsing three times with deionized H₂O for 5 min each time, the samples were stained for 2 h with 2% uranyl acetate in maleate buffer, pH 5.4. At the end of the staining steps, the samples were rinsed three times with deionized H₂O for 5 min each time.

ESEM, FIB-Tomography, and Microanalysis

Hydrated hydrogel scaffold samples were placed on aluminum SEM stubs and transferred to a vacuum chamber. ESEM, FIB/SEM, and microanalysis were performed using Quanta DualBeam 3D (FEI company, Hillboro, OR) and Helios 600 instrument (FEI company). Low vacuum mode was first selected for the investigations, and sample images were acquired at room temperature with pressure equilibrium achieved at approximately 50 Pa. For the other analyses with high vacuum requirements, samples after freeze-drying were first fractured using a razor blade to expose the interior regions and then positioned on SEM stubs with double-sided carbon tape. Sputter coating with gold to a thickness of approximately 10 nm was performed to reduce charging effects during beam irradiation. The samples were transferred and kept in high vacuum mode for all the imaging and analysis. For elemental analysis based on EDS, aliquots were prepared using the same freezing and drying procedures without the staining procedures, and coating with Au or Pt was not performed to avoid signal bias. EDS acquisition was

based on the Pegasus X-ray analysis system (EDAX) with a Si drift detector.

Measurement of Pore Size and Scaffold Porosity

The pore size and porosity of hydrogel scaffold samples were obtained from FIB-tomography and LSCM analysis, with details presented in the Results. For comparison, measurements were also carried out using mercury porosimetry with an AutoPore II 9220 instrument (Micromeritics, Norcross, VA) to determine pore size distributions, median pore diameter, and porosity. A solid penetrometer volume ranging from 6.7 to 7.3 mL and samples weighing about 0.1 g were used. Mercury was filled from a filling pressure of 3.4 kPa (0.5 psi) and intruded to a maximum pressure of 414 MPa (60,000 psi). The three-phase contact angle between the liquid (mercury), vapor and the surface (polymer) was 137 ± 1 ($n=4$) degree, and this was used to calculate the pore diameter from the intrusion pressure.

Correlative Imaging with Light and Electron Microscopy

To construct an artificial environment to mimic the porous hydrogel membrane, thin layer of Gtn-HPA/CMC-Tyr hydrogel was coated on silicon nitride membrane windows (Silson Ltd, Northampton, England) by spin coating (Laurell Technologies Corporation, North Wales, PA, model number WS-400). The thickness of the hydrogel layer was controlled at approximately $1 \mu\text{m}$ uniformly, to allow large area cell growth for high throughput analysis. The window was then placed in petri dish with culture medium, and COS-7 cells were seeded until expected confluence achieved. The thickness of the silicon nitride membrane was 500 nm, which allows routine light microscopy and confocal imaging performed on the cells attached to the membrane portion. Staining procedures for confocal and SEM imaging, as presented in previous sections, were also applied, and no detectable damage or change was found on the membrane or the hydrogel layer. For final SEM imaging, postfixation was carried out for 20 min in 1:1 osmium tetroxide 2% stock in 0.2 M sodium cacodylate with 4 mM CaCl_2 . The device was then washed in 0.1 M sodium cacodylate in 2 mM CaCl_2 in distilled water for 10 min to remove excess osmium tetroxide, and air dried followed by transferring to SEM.

Results

Imaging Results

Gtn-HPA/CMC-Tyr hydrogel was selected as a model porous scaffold for this nanocharacterization study, and the characteristic of this hydrogel will be presented elsewhere. Cell growth inside the Gtn-HPA/CMC-Tyr scaffolds was

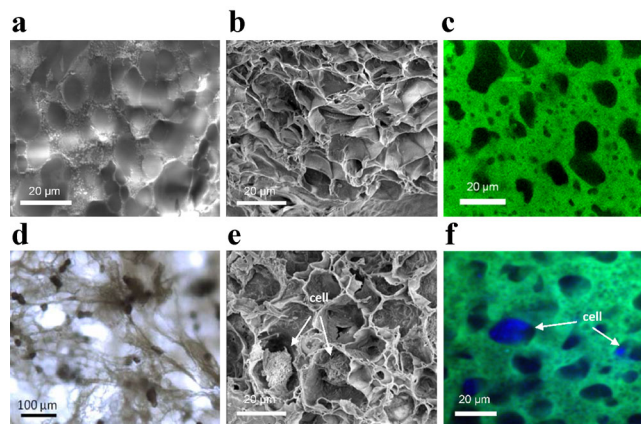


Figure 1. Images of Gtn-HPA/CMC-Tyr hydrogel scaffold using routine approaches. **a:** ESEM image of the hydrogel surface in a hydrated state; **(b)** SEM image of the sample in **(a)** after freeze-drying; **(c)** LSCM image of hydrogel scaffold with FITC labeling; **(d)** photomicrograph of cells in hydrogel scaffold; **(e)** SEM image of cells in hydrogel scaffold; and **(f)** LSCM image of FITC-labeled hydrogel scaffold with cells stained with DAPI.

first investigated by routine approaches including light microscopy, conventional SEM, and confocal microscopy. The results are presented in Figure 1a–c for hydrogel scaffold samples without cells and in Figure 1d–f for hydrogel scaffold samples with cells. Light microscopy and confocal microscopy are two efficient approaches for initial investigation of cell growth, including viability, but the resolution is limited and only the rough shape of the cells could be interpreted. After freeze-drying of the samples, cell growth on the top surfaces could be located by SEM (Fig. 1e) with fine details. However, the interaction volume of the incident electrons gives a penetration depth in the micrometer scale so that the structures underneath, including interconnected microstructures and their contact with the cells, could not be characterized.

Coupled with the capability of high precision material removal by FIB, characterization can now be performed on cells inside hydrogel scaffold structures. After imaging the cell-seeded hydrated sample with ESEM, the chamber was pumped down to high vacuum mode ($\sim 10^{-3}$ Pa). With 15 min drying time, the vacuum-dried samples became suitable for routine SEM. Some areas with exposed cells were further investigated by EDS imaging to acquire the chemical signals. The results are shown in Figure 2a containing the major identified elements (Cl, Na, O, and P). The last image of Figure 2a shows an overlay of Cl, O, and P, and the high concentration of cell rich O and P in contrast to the scaffold's Cl confirms the presence of cells inside the hydrogels. In addition, stained and freeze-dried aliquots were also imaged. A partially covered cell shown in Figure 2b and surrounding microstructures were sectioned by FIB milling to expose the interfaces (see Fig. 2c), and a high magnification SEM image (Fig. 2d) with pixel size of

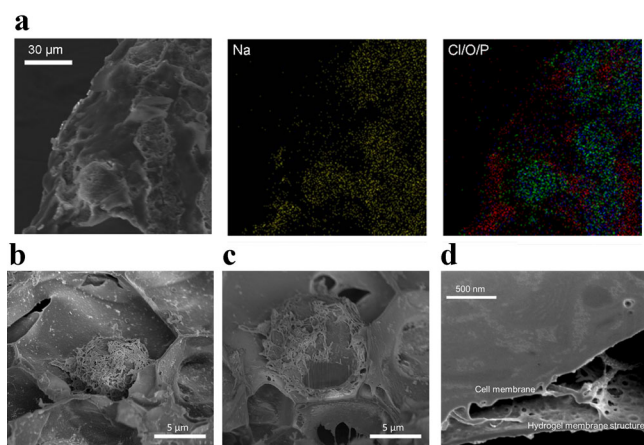


Figure 2. Imaging cells in hydrogel with ion and electron beams. **a:** SEM-EDS image of exposed cells with EDS image of Na, and overlay of Cl (red), O (blue) and P (green). SEM imaging of a cell grown partially in hydrogel scaffold (**b**) before, and (**c**) after FIB milling. **d:** High magnification SEM image of the cell–hydrogel interface.

2 nm was acquired to reveal the details of the cell–hydrogel interface.

3D Reconstruction of Cells in Hydrogel Scaffold

In addition to exposing the interfaces of cells grown in hydrogel scaffold as shown in Figure 2d, we further demonstrate the capability of FIB-tomography in capturing cell growth inside hydrogel scaffolds in true three dimensions. The regions of interest were first identified by low magnification SEM, and a platinum-based conductive layer of thickness 500 nm was deposited by a chemical vapor deposition (CVD) process on the top surface to minimize charging and channeling effects during ion beam milling. FIB and SEM were applied alternately to acquire the serial sectioned images: the automatic control was based on the “Slice-and-View” software package from the manufacturer (FEI company). Two 3D stacks were obtained at different magnifications, and the detailed process parameters are presented in Table I. In the first 3D stack showing cells in hydrogel scaffold, cell growth was captured with the surrounding hydrogel scaffold microstructures, and characteristics such as porosity were determined subsequently. The second stack which focused on cell–hydrogel interfaces was performed at high magnification with a pixel size of

2.5 nm to visualize the 3D interfaces; the slice thickness was also controlled precisely at 20 nm.

The beam current of a 30 kV Ga ion beam was set to 1–2 nA and, for SEM imaging, electron signals were acquired using a secondary electron (SE) detector or a mixed mode of SE and backscattering electron (BSE) signals. Imaging distortion due to the stage tilting to 52° was corrected by the “tilt correction” function provided in manufacturer’s software. Upon completion of the data acquisition, misalignment due to stage drift or charging was corrected by cross correlation techniques and extra regions not exposed to FIB milling were cropped before reconstruction. The surface reconstruction was achieved with Amira software package (Visage Imaging, Richmond, Australia) installed in a high performance computing facility with interested regions segmented.

The results of the first 3D stack for tomography of cells in hydrogel scaffold are presented in Figure 3a, and a movie of the serial images is presented in Supplementary Material 1. The field of view was set to approximately 100 μm to visualize a wide range of hydrogel microstructures. No significant “curtaining” effects could be observed throughout the image stack, as a result of stage stability and the protective platinum coating on top of the sample. Two cells growing inside the hydrogel scaffold were captured as indicated by the arrows in Figure 3a. After identifying the hydrogel structures with the segmentation tools in Amira, the final surface of the imaged scaffold was computed by the built-in surface generation function in Amira. Due to the complexity of porous structures, the result contained a large number of triangles (approximately 10,000,000) to provide a detailed model which was presented in Figure 3b. One advantage of FIB-tomography is the ability to obtain information such as porosity for microstructures. Pore size measurements were performed on the hydrogel scaffolds based on the results from FIB-tomography and LSCM with ImageJ software (National Institutes of Health). Random areas were selected from the original images to minimize the bias from local regions. The average diameters of the identified pores were measured for multiple times across the image or the image stack. The porosity was estimated after thresholding to include the pores only, and the percentage of blank pixel was considered as the porosity. The calculated results, together with measurements obtained using mercury porosimetry, are presented in Figure 4a and b.

The results for mean pore size revealed by FIB-tomography, LSCM, and mercury porosimetry confirmed

Table I. Parameters of the data acquisition processes for 3D visualization of cells in hydrogel.

3D stack	Number of images acquired	Volume dimensions (μm)	Slice thickness (nm)	Pixel size (nm)	Electron beam voltage (kV)	Beam dwell time (ms)
Tomography of cells in hydrogel scaffold	137	84 × 70 × 17	125	50	10	30

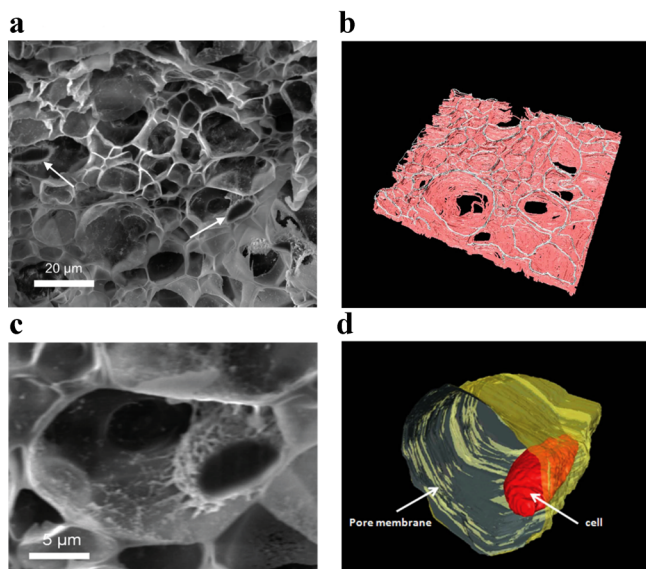


Figure 3. Representative image shows FIB/SEM 3D tomography of cells in hydrogel scaffold. **a:** A single slice from the 3D image stack showing two cells (indicated by arrows) and the surrounding hydrogel structures sectioned by FIB. **b:** Surface reconstruction of the volume ($84 \times 70 \times 17 \mu\text{m}^3$ from 137 images) containing 10 million triangles based on FIB/SEM tomography showing the hydrogel scaffold microstructures. **c:** A single image in the FIB/SEM tomography image stack showing a cell with the surrounding hydrogel sectioned by FIB milling, and **(d)** the corresponding 3D reconstruction (total 137 images) showing the cell (red) grown in the single hydrogel pore (yellow).

the presence of macroporous structures in the Gtn-HPA/CMC-Tyr samples. Based on all three methods, the pore size measured was in the range of 10–50 μm . The mean pore sizes based on FIB-tomography and LSCM were found to be 21 and 19 μm , respectively, reflecting the consistency of pore size measurement using these two direct imaging approaches. In FIB-tomography, the hydrogel sample may have reduced membrane thickness for each pore with architecture remained, and thus slightly larger pore size was reported compared to LSCM measurement performed in fully hydrated state. However, the mean pore size obtained by mercury porosimetry was significantly larger compared to those by FIB-tomography and LSCM, with $P < 0.01$ obtained from two sample *z*-test. High porosity values larger than 50% were obtained based on all the three approaches, and significant difference of measures was found ($P < 0.01$) in each pair of the three approaches, with maximum from mercury porosimetry and minimum from LSCM.

The results show that pore measurements by FIB-tomography and LSCM are comparable, and can be used jointly to determine the hydrogel scaffold properties. The porosity measured by LSCM can be lower compared to FIB-tomography, implying the water contents in the samples prepared for LSCM may prevent some of the pores to be observed. Measurements of pore size and porosity by mercury porosimetry can result in significantly larger values compared to those based on FIB-tomography and LSCM.

The discrepancy may be due to the fact that FIB-tomography and LSCM methods provide local measurements, whereas mercury porosimetry measures a large portion or the whole sample. Therefore, it should be suggested that if localized information is preferred in future studies, microscope-based methods are obviously advantageous. And mercury porosimetry will provide the overall characteristics of the target sample. Difference in porosity can be expected which is dependent on the measurement method and other factors such as sample homogeneity.

The membrane-type hydrogel structures were evident in the acquired images, and in addition, the reconstructed 3D model can provide a unique way to locally explore the interconnectivity or the surface area of the hydrogel structures. With FIB-tomography, two cells grown in the hydrogel scaffold were captured in 3D as indicated by the arrows in Figure 3a, and the pores with the residing cells can be compared directly with the other surrounding pores. Reconstruction of one target cell with surrounding hydrogel membrane is presented in Figure 3c and d. For the specific two pores, measurements of the pore size were performed by ImageJ on both the short and long axes of the ellipsoidal shape pores, and multiple readings were taken through the 3D stack. The average size for the pores with cells inside is 18 μm , consistent with the average pore size $21 \pm 8.9 \mu\text{m}$ obtained from all the images acquired.

We further built a prototype platform for correlative imaging with both light and electron microscopy based on silicon nitride membrane of submicron thickness as illustrated in Figure 5a. The hydrogel material to investigate can be spin coated onto the silicon nitride membrane with controlled thickness to be light transparent. Light microscopy and confocal imaging can then be performed to study the cells growth on this artificial environment in a potentially high throughput setup. With FA and DAPI staining, the results of confocal imaging were presented in Figure 5b, showing the monolayer of cells growing on the hydrogel layer with distinct distribution of the FAs. After postfixation and dehydration, SEM imaging was also performed on the same sample as shown in Figure 5c, revealing that the growing cells were in close contact or even partially inside the hydrogel.

Discussion

Characterization of cells inside a 3D matrix, particularly at high magnification, is an essential but challenging task. FIB is by far the most promising method with the capability to investigate target volumes with dimensions of tens of micrometers. With spot size approaching single digit nanometer values and sufficient rates of material removal, FIB allows physical separation of any target material with nanometer precision. Coupled with numerous analytical tools, FIB-tomography is becoming the ideal tool for probing cells and surrounding microstructures to obtain structural and compositional information. In this study, we

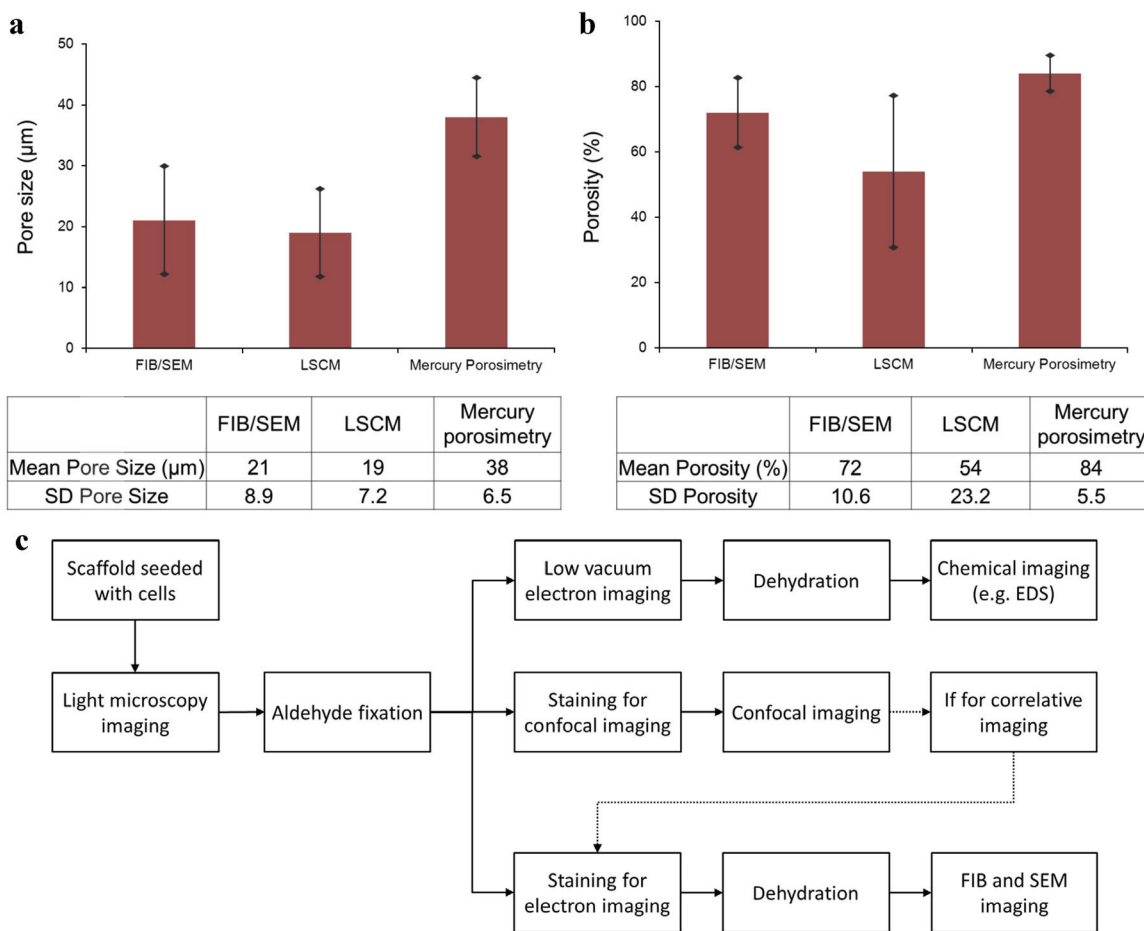


Figure 4. Comparison of the results from FIB/SEM, LSCM and Mercury porosimetry in terms of measuring (a) pore size and (b) porosity of the Gtn-HPA/CMC-Tyr samples. c: Summary of the sample preparation processes for investigating cells in hydrogel scaffold.

first demonstrated that FIB and associated tools can effectively enable analyses of 3D cell-materials interfaces, which are crucial for novel biomaterial design but cannot be acquired easily by other methods. With the protocols developed, the water content of the injectable hydrogels was slowly released in freeze-drying cycles so that the microstructures could be properly preserved without significant morphological change. Embedding or chemical fixation is not necessary in this approach, and high resolution compositional mapping becomes feasible. With the ever-increasing application of hydrogel scaffolds and other porous biomaterials, the acquired structural and chemical information for both cells and materials has additional implications for material design relevant to cell growth.

More importantly, cells grown inside hydrogel scaffolds can be simultaneously imaged and analyzed. This unique correlated information is invaluable not only for materials design but also for understanding processes of cell proliferation, migration, and differentiation inside matrices. The staining protocols used here were derived from those

used extensively in TEM, with revisions to accommodate the imaging mechanisms which are dominated by BSEs (Heymann et al., 2009; Leser et al., 2009). Protein localization is also viable with routine antibody conjugated nanoprobe or correlative imaging (Murphy et al., 2011). Although Pt coating is only performed on top of the target hydrogel sample, curtaining effect was not observed on the sectioned surfaces of the cells inside. It is likely for FIB milling of thin membranes, the removal process is highly efficient, and thus the structural inhomogeneity is negligible.

With the results from both confocal and SEM imaging presented in Figure 5, it can be concluded that at this time point, the FAs are anchored on or inside the hydrogel layer. Herein we demonstrate the same sample, with proper device and fixations, can be correlated with both light and electron microscopy. The proteins involved in cell mobility can be then directly mapped to the surrounding materials. As the thickness of the hydrogel layer is tunable in the coating process, the proposed approach will be flexible to host a

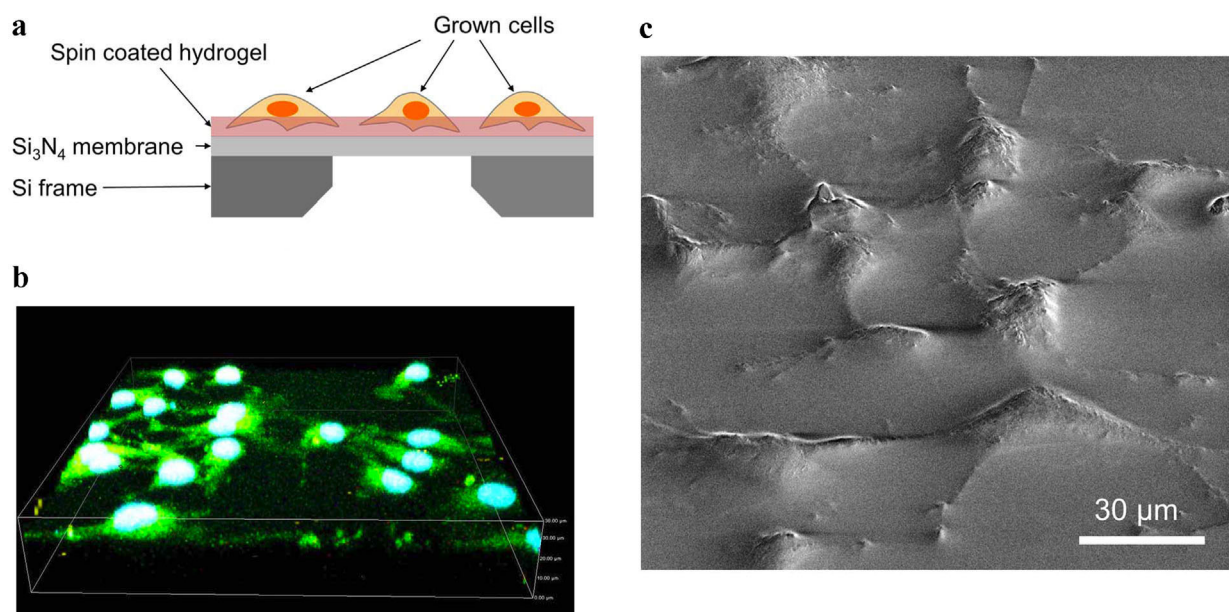


Figure 5. Proposed silicon membrane based platform for correlative imaging of cell growth with novel biomaterials (a) the schematic diagram of the device with spin coated hydrogel layer, and the cells can be seeded on top. b: With focal adhesion and DAPI staining, confocal imaging reveals the FAs and nuclei of the monolayer COS-7 cells grown on the hydrogel layer, and (c) SEM imaging of the same sample showing the cells partially immersed in the hydrogel layer with morphology preserved.

wide range of novel materials for correlative cell growth investigation.

It should be noted that investigations enabled by FIB typically target a volume which is less than 100 μm below the sample surface, and interaction volume of SEM is in the scale of a few micrometers. Additional fracturing such as cutting by razor blade is necessary to expose large interior regions, followed by cleaning by FIB cross-sectioning. Although preliminary results have been shown in this study, imaging complete cellular ultrastructures during growth in hydrogel scaffold is dependent on multiple factors: (i) specification of the optics, (ii) additional staining necessary to induce sufficient contrast between various organelles and membrane structures, and (iii) effectiveness of immobilization. For the first two factors, current low voltage SEM images, supported by both secondary and BSEs, are soon to match TEM images in terms of beam spot size and contrast. Some discussions on staining protocols have already been conducted for increasing contrast, particularly for BSEs (Heymann et al., 2009; Leser et al., 2009). The third factor, effective immobilization of hydrated samples without structural damage, is expected to be a major hurdle, as both the cells and hydrogel are water-rich but varied in concentration levels. Freezing is well known for inducing ice crystal damage to cellular structures or morphology if the freezing rate is not sufficiently high, and some damages can be recognized in Figure 2d. One possible solution is high pressure freezing (HPF) which provides close to native state of cryo sample fixation. Cryogenic FIB (Cryo-FIB) and SEM (Cryo-SEM) (Fu et al., 2008a; Marko et al., 2007; Mcgeoch,

2007) may be the ultimate approach to study cells in matrices, considering the advantages of close-to-native status and the ultrahigh speed of material removal (Fu et al., 2008b; Marko et al., 2007). Continuous development is still on-going (Hayles et al., 2007, 2010; Rigort et al., 2010) and characterization of cells in hydrogel scaffold conducted in a cryogenic environment, together with correlative imaging, will be a subject of future study.

The authors would like to acknowledge support from the New Staff Member Research Fund from the Faculty of Engineering, Monash University. Funding for this work was partly provided through Australian Research Council Discovery (ARC) Project Grant DP 120102570 and DP 120100583. This work was performed in part at the Monash Centre of Electron Microscopy (MCEM) and the Melbourne Centre for Nanofabrication (MCN), an initiative partly funded by the Commonwealth of Australia and the Victorian Government. High performance computing was supported by Multi-modal Australian Sciences Imaging and Visualisation Environment (MASSIVE). The authors also thank Dr. Manoj Sridhar, Mr. David Vowles, and Monash Microimaging for experiment assistance.

References

- Bennett AE, Narayan K, Shi D, Hartnell LM, Gousset K, He H, Lowekamp BC, Yoo TS, Bliss D, Freed EO, Subramaniam S. 2009. Ion-abrasion scanning electron microscopy reveals surface-connected tubular conduits in HIV-infected macrophages. *PLoS Pathogen* 5(9):e1000591.
- Bittermann AG, Burkhardt C, Hall H. 2009. Imaging of cell-to-material interfaces by SEM after in situ focused ion beam milling on flat surfaces and complex 3D-fibrous structures. *Adv Eng Mater* 11(11):B182–B188.

- da Silva J, Lautenschläger F, Sivaniah E, Guck JR. 2010. The cavity-to-cavity migration of leukaemic cells through 3D honey-combed hydrogels with adjustable internal dimension and stiffness. *Biomaterials* 31(8):2201–2208.
- Edwards HK, Fay MW, Anderson SI, Scotchford CA, Grant DM, Brown PD. 2009. An appraisal of ultramicrotomy, FIBSEM and cryogenic FIBSEM techniques for the sectioning of biological cells on titanium substrates for TEM investigation. *J Microsc* 234(1):16–25.
- Felts RL, Narayan K, Estes JD, Shi D, Trubey CM, Fu J, Hartnell LM, Ruthel GT, Schneider DK, Nagashima K, Bess JW, Bavari S, Lowekamp BC, Bliss D, Lifson JD, Subramaniam S. 2010. 3D visualization of HIV transfer at the virological synapse between dendritic cells and T cells. *Proc Natl Acad Sci* 107(30):13336–13341.
- Ford MC, Bertram JP, Hynes SR, Michaud M, Li Q, Young M, Segal SS, Madri JA, Lavik EB. 2006. A macroporous hydrogel for the coculture of neural progenitor and endothelial cells to form functional vascular networks in vivo. *Proc Natl Acad Sci USA* 103(8):2512–2517.
- Friedmann A, Cismak A, Tautorat C, Koester PJ, Baumann W, Held J, Gaspar J, Ruther P, Paul O, Heilmann A. 2011a. FIB preparation and SEM investigations for three-dimensional analysis of cell cultures on microneedle arrays. Scanning DOI: 10.1002/sca.20297.
- Friedmann A, Hoess A, Cismak A, Heilmann A. 2011b. Investigation of cell-substrate interactions by focused ion beam preparation and scanning electron microscopy. *Acta Biomater* 7(6):2499–2507.
- Fu J, Joshi S, Catchmark JM. 2008a. A study of angular effects in focused ion beam milling of water ice. *J Micromech Microeng* 18(9):095010.
- Fu J, Joshi SB, Catchmark JM. 2008b. Sputtering rate of micromilling on water ice with focused ion beam in a cryogenic environment. *J Vac Sci Technol A* 26(3):422–429.
- Giannuzzi LA, Stevie FA. 2005. Introduction to focused ion beams: Instrumentation, theory, techniques, and practice. New York: Springer. xiv, p 357.
- Greulich C, Diendorf J, Simon T, Eggeler G, Eppler M, Köller M. 2011. Uptake and intracellular distribution of silver nanoparticles in human mesenchymal stem cells. *Acta Biomater* 7(1):347–354.
- Hayles MF, Stokes DJ, Phifer D, Findlay KC. 2007. A technique for improved focused ion beam milling of cryo-prepared life science specimens. *J Microsc* 226(3):263–269.
- Hayles MF, Matthijs de Winter DA, Schneijdenberg CTWM, Meeldijk JD, Luecken U, Persoon H, de Water J, de Jong F, Humbel BM, Verkleij AJ. 2010. The making of frozen-hydrated, vitreous lamellas from cells for cryo-electron microscopy. *J Struct Biol* 172(2):180–190.
- Heymann JAW, Hayles M, Gestmann I, Giannuzzi LA, Lich B, Subramaniam S. 2006. Site-specific 3D imaging of cells and tissues with a dual beam microscope. *J Struct Biol* 155(1):63–73.
- Heymann JAW, Shi D, Kim S, Bliss D, Milne JLS, Subramaniam S. 2009. 3D Imaging of mammalian cells with ion-abrasion scanning electron microscopy. *J Struct Biol* 166(1):1–7.
- Hildebrand M, Kim S, Shi D, Scott K, Subramaniam S. 2009. 3D imaging of diatoms with ion-abrasion scanning electron microscopy. *J Struct Biol* 166(3):316–328.
- Hollister SJ. 2005. Porous scaffold design for tissue engineering. *Nat Mater* 4(7):518–524.
- Jin R, Moreira Teixeira LS, Dijkstra PJ, van Blitterswijk CA, Karperien M, Feijen J. 2010. Enzymatically-crosslinked injectable hydrogels based on biomimetic dextran—Hyaluronic acid conjugates for cartilage tissue engineering. *Biomaterials* 31(11):3103–3113.
- Keskar V, Marion NW, Mao JJ, Gemeinhart RA. 2009. In vitro evaluation of macroporous hydrogels to facilitate stem cell infiltration, growth, and mineralization. *Tissue Eng Part A* 15(7):1695–1707.
- Knott G, Marchman H, Wall D, Lich B. 2008. Serial section scanning electron microscopy of adult brain tissue using focused ion beam milling. *J Neurosci* 28(12):2959–2964.
- Lee BH, West B, McLemore R, Pauken C, Vernon BL. 2006. In-situ injectable physically and chemically gelling NIPAAm-based copolymer system for embolization. *Biomacromolecules* 7(6):2059–2064.
- Lee F, Chung JE, Kurisawa M. 2008. An injectable enzymatically crosslinked hyaluronic acid-tyramine hydrogel system with independent tuning of mechanical strength and gelation rate. *Soft Matter* 4(4):880–887.
- Leser V, Drobne D, Pipan Z, Milani M, Tatti F. 2009. Comparison of different preparation methods of biological samples for FIB milling and SEM investigation. *J Microsc* 233(2):309–319.
- Li J, Stein D, McMullan C, Branton D, Aziz MJ, Golovchenko JA. 2001. Ion-beam sculpting at nanometre length scales. *Nature* 412(6843):166–169.
- Lucille AG, Daniel P, Nicholas JG, Mario JC. 2007. Two-dimensional and 3-dimensional analysis of bone/dental implant interfaces with the use of focused ion beam and electron microscopy. *J Oral Maxillofac Surg* 65(4):737–747.
- Marko M, Hsieh C, Schalek R, Frank J, Mannella C. 2007. Focused-ion-beam thinning of frozen-hydrated biological specimens for cryo-electron microscopy. *Nat Methods* 4(3):215–217.
- Martínez E, Engel E, López-Iglesias C, Mills CA, Planell JA, Samitier J. 2008. Focused ion beam/scanning electron microscopy characterization of cell behavior on polymer micro-/nanopatterned substrates: A study of cell-substrate interactions. *Micron* 39(2):111–116.
- McGeoch JEM. 2007. Topology of the mammalian cell via cryo-FIB etching. *J Microsc* 227(2):172–184.
- Murphy GE, Narayan K, Lowekamp BC, Hartnell LM, Heymann JAW, Fu J, Subramaniam S. 2011. Correlative 3D imaging of whole mammalian cells with light and electron microscopy. *J Struct Biol* 176(3):268–278.
- Nehrer S, Breinan HA, Ramappa A, Young G, Shortkroff S, Louie LK, Sledge CB, Yannas IV, Spector M. 1997. Matrix collagen type and pore size influence behaviour of seeded canine chondrocytes. *Biomaterials* 18(11):769–776.
- Rigort A, Bauerlein FJB, Leis A, Gruska M, Hoffmann C, Laugks T, Böhm U, Eibauer M, Gnaegi H, Baumeister W, Plitzko JM. 2010. Micromachining tools and correlative approaches for cellular cryo-electron tomography. *J Struct Biol* 172(2):169–179.
- Schroeder-Reiter E, Perez-Willard F, Zeile U, Wanner G. 2009. Focused ion beam (FIB) combined with high resolution scanning electron microscopy: A promising tool for 3D analysis of chromosome architecture. *J Struct Biol* 165(2):97–106.
- Volkert CA, Minor AM. 2007. Focused ion beam microscopy and micro-machining. *MRS Bull* 32:389–395.
- Wang L-S, Chung JE, Pui-Yik Chan P, Kurisawa M. 2010. Injectable biodegradable hydrogels with tunable mechanical properties for the stimulation of neurogenesis differentiation of human mesenchymal stem cells in 3D culture. *Biomaterials* 31(6):1148–1157.